Infinite Science Publishing

Proceedings Article

Investigating the Harmonic Dependence of MPI Resolution

Mark-Alexander Henn [a,b] · Thinh Q. Bui [a,*] · Solomon I. Woods [a]

[a] National Institute of Standards and Technology (NIST), Gaithersburg, MD 20899, USA
[b] University of Maryland, College Park, MD 20742, USA
*Corresponding author, email: thinh.bui@nist.gov

Abstract

In this work we investigate how the MPI resolution changes as a function of signal harmonics. Based on a simulation study that models a lock-in measurement of the point spread function we apply our findings to actual measurement data obtained from NIST's MPI instrument. In both cases we show that the image resolution improves by a factor of more than two between the 3rd and 7th harmonic.

I. Introduction

The application of magnetic particle imaging (MPI)[1–3] to temperature estimation has highlighted the value of accurately measuring the harmonics or ratios of the harmonics of a time-domain MPI signal [4]. Using lock-in amplifiers [5] is a way to measure these harmonics with high accuracy. The harmonic dependency of the system function for the system matrix approach and how the system function relates to Chebyshev polynomials has been investigated in [6].

In this work we investigate possible benefits from limiting the signal to certain harmonics for the imaging process. In contrast to the system matrix approach that usually requires the full harmonic spectrum of the measured MPI signal to be taken into consideration, X-space [7, 8] and especially low velocity X-space measurements can be modified to only use specific harmonics. The spatial resolution of such a measurement is directly related to the full width at half maximum (FWHM) of the point spread function (PSF) as shown in [8].

We therefore perform a simulation study of a lock-in measurement of the PSF harmonics, determine the change in the PSF's FWHM, and apply our findings to measurement data obtained from NIST's MPI instrumen-

tation [9]. It turns out that a more than fourfold improvement in resolution can be achieved by going to higher harmonics.

II. Methods

In order to determine the resolution we follow an approach similar to [8] to generate the PSFs. We then fit a Gaussian distribution with standard deviation σ to the obtained PSFs and estimate the FWHM using that FWHM $\approx 2.355 \cdot \sigma$.

II.I. Signal Generation

The time-dependent PSF in the general n-dimensional case can be modeled as:

$$\vec{u}(t) = \frac{d}{dt} \vec{M}[\vec{H}(t)], \tag{1}$$

with

$$\vec{M}(\vec{H}) = m\mathscr{L}(k\vec{H})\frac{\vec{H}}{||\vec{H}||}, \text{ and } k = \frac{\mu_0 m}{k_B T}, \tag{2}$$

Table 1: Simulation Parameters.

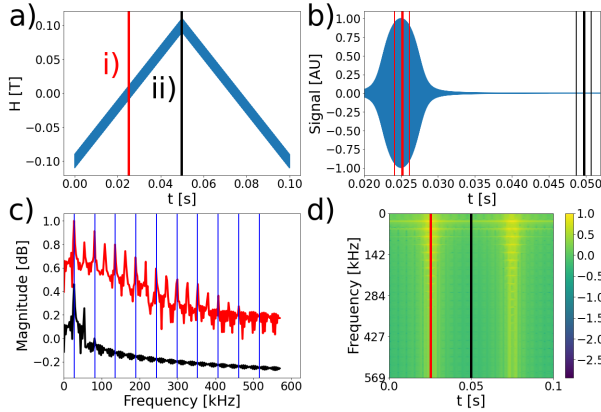| Parameter	Symbol	Value
Particle Diameter	d	$2 \cdot 10^{-8}$ m
Saturation Magnetization	M_s	$4.5 \cdot 10^5$ A/m
Temperature	T	300 K
Excitation Field Frequency	f_1	27.125 kHz
Bias Field Frequency	f_0	10 Hz
Excitation Field Amplitude	H_1	10 mT
Bias Field Amplitude	H_0	100 mT

Figure 1: (a) The applied field as a function of time, the red line i) denotes the time when the bias field is zero, the black line ii) denotes the time when the bias field is at its maximum, (b) zoomed-in view of the particle response at positions i) and ii) with thin lines marking the integration times. (c) Fourier spectrum calculated at the two different times in (b), red for i), black for ii), the blue vertical lines denote the odd harmonics. (d) spectrogram of the lock-in simulation for different center points of integration using a triangular shaped window function that results in a 50% overlap in the integration domain.

here m is the magnetic moment of a single particle, that is itself a function of the saturation magnetization M_s and the particle diameter d, and $\mathcal{L}$ is the Langevin function.

We assume the one-dimensional case in which the drive field is a combination of a scalar bias field with low frequency f_0 and amplitude H_0 and a scalar excitation field with amplitude H_1 and high frequency f_1, such that:

$$H(t) = -H_0 + \frac{2H_0}{\pi}\arccos\left[\cos\left(2\pi f_0 t\right)\right] + H_1\sin\left(2\pi f_1 t\right). \quad (3)$$

II.II. Lock-in Calculation.

A lock-in amplifier works by mixing the input signal $u(t)$ with a reference signal and then integrating the resulting signal over a small time window ($\Delta_t \approx 0.001$ s), potentially also applying a weighting function $w(t)$ over the integration time window, such as a simple triangle, a Hamming or a Hann window [10]. In any case the lock-in
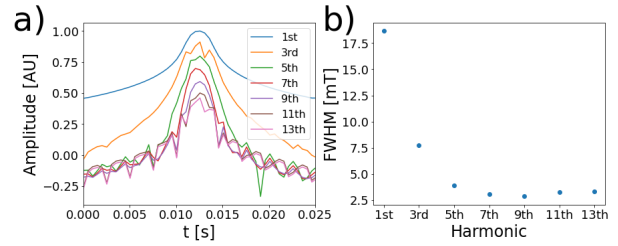

Figure 2: (a) The harmonics of the PSF obtained from the lock-in simulations for the 1st to 13th harmonic. (b) The FWHM values for each of those harmonics obtained by fitting a Gaussian distribution.

simulation amounts to calculating:

$$\hat{u}(t, k) = \int_{t-\Delta_t/2}^{t+\Delta_t/2} w(\tau)u(\tau)\exp(-2i\pi k f_1 \tau)d\tau, \quad (4)$$

effectively calculating the k-th harmonic of $u(t)$, i.e., the k-th harmonic of the PSF.

III. Results

Figure 1 shows the applied field, the resulting $u(t)$, and its harmonics for the parameter values given in Table 1, assuming a Langevin particle response.

III.I. Changes in the FWHM

From Figure 2 we see that the FWHM decreases for the higher harmonics. Also, at any point in time, the contribution to the signal decreases monotonically with increasing harmonic number.

The change in the FWHM with harmonic number can be explained by looking at the M vs. H curves at different times as shown in Figure 3. We see that if we move away from the time at which the bias field is at its minimum and the signal is strongest, i.e., the red line in Figs. 1 and 3, the signal becomes closer to a linear signal. Thus, the higher harmonics of the PSF will decay faster for times away from the peak signals in Figure 2 (b), leading a to smaller FWHM for the higher harmonics.

Estimating the change in the FWHM quantitatively by fitting Gaussian distributions to the harmonics of the PSF shows that the resolution dramatically improves for the higher harmonics, as shown in Fig. 2 (b), where we go from a FWHM of around 18 mT for the first harmonic to 8.4 mT for the third harmonic and 3.2 mT for the 11th harmonic.

III.II. Reconstruction from Measurements

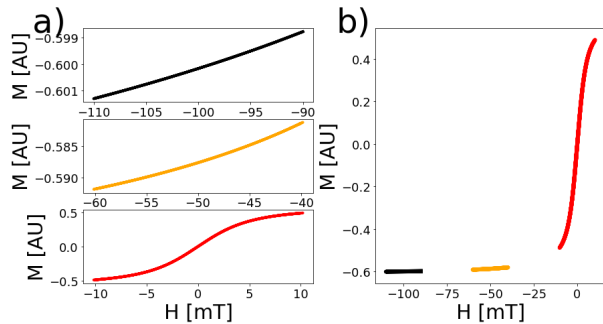In a last step, we look at the harmonic dependence of measurement data from NIST's MPI instrumenta-

Figure 3: Detail of the PSF simulation for a bias field with H_0=100 mT, f_0=10 Hz, and excitation field with H_1=10 mT, f_1=27.125 kHz. The line colors correspond to the colors used in Fig. 1, i.e., the times when the bias field is at its minimum (red) and maximum (black), with the yellow line being in between the black and red lines. (a) Individual M vs. H curves, (b) M vs. H curves plotted together. Note, that the M vs. H behaviour more closely reflects a linear relationship as we approach the applied field values that are close to saturation, i.e., going from red to yellow to black.
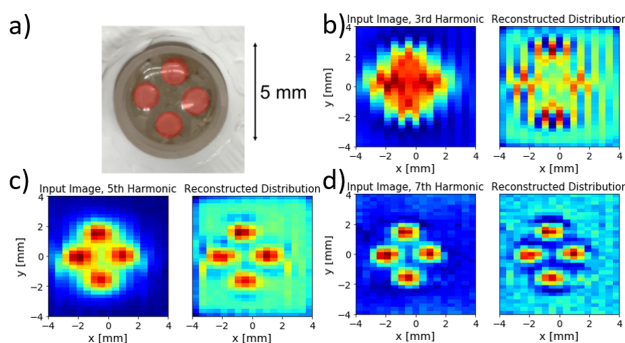

Figure 4: (a) Image of the measured phantom, MNPs are located in the four bubbles shaded red, (b-d) 2D-MPI image (left) and reconstructed particle distribution (right) for the 3rd harmonic, the 5th harmonic and the 7th harmonic. Note, the significantly improved resolution for the higher harmonics.

tion [9]. The data were obtained using a pixel by pixel scan of a Vivotrax tracer with a spatial resolution phantom made of glass, see Figure 4 (a). The experimental data were acquired using a drive field with $H_1 = 10$ mT, $f_1 = 27.125$ kHZ, and a gradient field with a gradient of 10 T/m in x-direction and 5 T/m in y/z-directions.

The particle concentration is determined by deconvolving the 2D-MPI image data using a Toeplitz matrix that accounts for the different harmonics of the PSF, as explained in more detail in [11]. The FWHMs for the different harmonics were based on the values determined by our simulations shown in Fig. 2 (b). As expected, we can see a clear improvement in the reconstruction using the higher harmonics, i.e., going from Fig. 4 (b) to (d).

IV. Conclusion

In this presentation we investigated the harmonic dependence of the MPI resolution by simulating a lock-in measurement of the PSFs higher harmonics. We found that the resolution can dramatically be improved by measuring these higher harmonics. These findings have been confirmed by analysing measurement data from NIST's MPI instrument, that lead to up to a fourfold improvement in spatial resolution.

Acknowledgments

Author's statement

Conflict of interest: Authors state no conflict of interest. Disclaimer: Reference is made to commercial products to adequately specify the experimental procedures involved. Such identification does not imply recommendation or endorsement by the National Institute of Standards and Technology, nor does it imply that these products are the best for the purpose specified.

References

[1] J. Weizenecker, J. Borgert, and B. Gleich. A simulation study on the resolution and sensitivity of magnetic particle imaging. *Physics in Medicine & Biology*, 52(21):6363, 2007.

[2] T. Knopp and T. M. Buzug, Magnetic Particle Imaging: An Introduction to Imaging Principles and Scanner Instrumentation. Berlin/Heidelberg: Springer, 2012, doi:10.1007/978-3-642-04199-0.

[3] N. Panagiotopoulos, R. L. Duschka, M. Ahlborg, G. Bringout, C. Debbeler, M. Graeser, C. Kaethner, K. Lüdtke-Buzug, H. Medimagh, J. Stelzner, *et al.* Magnetic particle imaging: Current developments and future directions. *International journal of nanomedicine*, 10:3097, 2015.

[4] J. B. Weaver, A. M. Rauwerdink, and E. W. Hansen. Magnetic nanoparticle temperature estimation. *Medical physics*, 36(5):1822–1829, 2009.

[5] Zurich Instruments. Principles of lock-in detection and the state of the art. *White Paper*, 2016, https://www.zhinst.com/americas/en/resources/principles-of-lock-in-detection.

[6] J. Rahmer, J. Weizenecker, B. Gleich, and J. Borgert. Signal encoding in magnetic particle imaging: Properties of the system function. *BMC medical imaging*, 9:1–21, 2009.

[7] P. W. Goodwill and S. M. Conolly. The X-space formulation of the magnetic particle imaging process: 1-D signal, resolution, bandwidth, SNR, SAR, and magnetostimulation. *IEEE transactions on medical imaging*, 29(11):1851–1859, 2010.

[8] P. W. Goodwill, E. U. Saritas, L. R. Croft, T. N. Kim, K. M. Krishnan, D. V. Schaffer, and S. M. Conolly. X-space MPI: magnetic nanoparticles for safe medical imaging. *Advanced materials*, 24(28):3870–3877, 2012.

[9] T. Q. Bui, M.-A. Henn, W. L. Tew, M. A. Catterton, and S. I. Woods, Temperature-dependent magnetic particle imaging with multi-harmonic lock-in detection, 2023. doi:10.48550/ARXIV.2301.08539.

[10] J. O. Smith, Spectral Audio Signal Processing. http://ccrma.stanford.edu/~jos/sasp/,

[11] M.-A. Henn, K. N. Quelhas, T. Bui, and S. Woods. Improving model-based MPI image reconstructions: Baseline recovery, receive coil sensitivity, relaxation and uncertainty estimation. *International Journal on Magnetic Particle Imaging*, 8(1), 2022.